Composites Part C: Open Access 5 (2021) 100155

Contents lists available at ScienceDirect

Composites Part C: Open Access

journal homepage: www.elsevier.com/locate/jcomc

# Study of structure morphology and layer thickness of $Ti_3C_2$ MXene with Small-Angle Neutron Scattering (SANS) ☆

Anthony Chun Yin Yuen [a,1,*], Timothy Bo Yuan Chen [a,1], Bo Lin [a], Wei Yang [a,b], Imrana I. Kabir [a], Ivan Miguel De Cachinho Cordeiro [a], Andrew E. Whitten [c], Jitendra Mata [c], Bin Yu [d], Hong-Dian Lu [b], Guan Heng Yeoh [a,c]

[a] School of Mechanical and Manufacturing Engineering, University of New South Wales, Sydney, NSW, 2052, Australia
[b] Department of Chemical and Materials Engineering, Hefei University, Hefei, Anhui, 230601, People's Republic of China
[c] Australian Centre for Neutron Scattering, Australian Nuclear Science and Technology Organisation (ANSTO), Lucas heights, NSW, 2234, Australia
[d] Centre for Future Materials, University of Southern Queensland, Toowoomba, QLD, 4350, Australia

ARTICLE INFO

*Keywords:*
MXene
Lamellar structure
SANS
SEM
XPS

ABSTRACT

MXene is a class of 2D materials exfoliated from ternary carbide and nitride ceramics. During synthesis, etching and delamination conditions affect the quality, overall crystallinity, defects and surface functionalization of MXene flakes. In this article, the morphological structure of MXene ($Ti_3C_2$) nanosheets under temperature between 20 °C and 60 °C were investigated with the application of Small-Angle Neutron Scattering (SANS) combined with several complementary techniques, such as Scanning Electron Microscopy (SEM) and Transmission Electron Microscopy (TEM) and X-ray Photoelectron Spectroscopy (XPS). The SANS analysis enabled structural information to be obtained about the $Ti_3C_2$ nanosheets, which consists of layers of transition metal carbides in a multilayer lamella morphology. The results showed that a single $Ti_3C_2$ layer is approximately 11.4 – 11.8 Å (1.14 – 1.18 nm) in thickness with a 20.3 – 21.5 Å (2.03 – 2.15 nm) interstacking layer gaps. This results in a total thickness of approximately 32 Å (3.2 nm), which was consistent with the model-dependent lamella model analysis. Furthermore, the thickness of the $Ti_3C_2$ layer increased by approximately ~2 Å (0.2 nm) when the temperature increased from 20 - 40 to 50 - 60 °C.

## 1. Introduction

Transition metal carbides, carbonites and nitrides (MXenes) are a family of two-dimensional (2D) layered material that have enormous potential applications due to their unique properties. MXenes and their hybrids containing small molecules, polymers or oxides are utilised as crucial materials in energy storage devices, including ion batteries, supercapacitors, and ion capacitors as well as hydrogen storage. MXenes are also highly desirable in EMI shielding due to their excellent flexibility, easy processing, and high conductivity with minimal thickness, having one of the highest EMI shielding effectiveness in terms of weight gain and thickness. The MXene field is rapidly growing, and to date, the MXene family includes more than 30 stoichiometric compositions, with many new MXene compositions and structures already under investigation [1]

MXene is produced by etching the "A" layer from MAX phases, a large family of ternary transition metal carbides, carbon nitrides and nitrides with a composition of $M_{n+1}AX_n$. As illustrated in **Fig. 1**, the M stands for early transition metal (such as Ti, V, Cr, Nb, etc.), A stands for a group A element (such as Al, Si, Sn, In, etc.), X stands for carbon and/or nitrogen, and n = 1, 2, or 3 [3]. There are many reports of MXene synthesis in the literature [4-6], but the etching processes are often carried out by immersing a MAX phase ($Ti_3AlC_2$) in hydrofluoric acid. The material is then exfoliated through sonication. The resulting MXene nanosheet ($Ti_3C_2$, thickness of around 1.2 - 1.8 nm) are functionalised through a surface modification using cationic surface active agents (CTAB and TBPB) [7,8]. Since MXenes are typically synthesized (derived) topochemically from their parent MAX phases via selective etching of the A element, the chemical composition and preparation protocol of the MAX phase affect the chemistry of the resultant MXene [4].

☆ Submitted to: Composites Part C: Open Access

* Corresponding author at: Centre Manager, ARC Training Centre for Fire Retardant Materials and Safety Technologies, School of Mechanical and Manufacturing Engineering, University of New South Wales, Sydney, NSW 2052, Australia
*E-mail address:* c.y.yuen@unsw.edu.au (A.C.Y. Yuen).

[1] Anthony Chun Yin Yuen and Timothy Bo Yuan Chen contributed equally to this work

https://doi.org/10.1016/j.jcomc.2021.100155
Received 29 December 2020; Received in revised form 7 April 2021; Accepted 4 May 2021

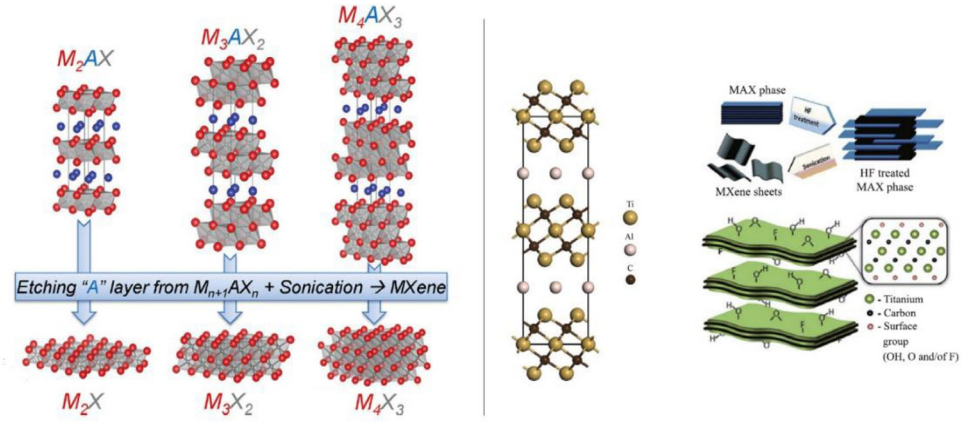


**Fig. 1.** Synthesis of MXenes from MAX phase $Ti_3AlC_2$.recreated from [2].

Furthermore, as-synthesized MXene flakes contain intrinsic defects [9,10] and the surface chemistry (which depends on etching conditions), intercalated species [11] and even the flake size [12] significantly affect MXene properties. Therefore, there is a growing need for detailed studies on the characterisation of as-synthesised and functionalised MXene. And thus provide a deeper understanding of MXene structure morphology, overall crystallinity, defects, surface functionalisation and how it is affected by the synthesis process.

Similar to MAX phase materials, MXene has a hexagonal close-packed structure where M atoms in MXenes are arranged in compact structures and X atoms fill the octahedral interstitial sites [3]. The atomic ordering of this structure is essential for the synthesis of MXene, as it significantly affects the properties and stability of the material [13,14]. Attractive electronic, magnetic, optical, plasmonic and thermoelectric properties have been predicted for many MXene through methods such as DFT [15] and molecular dynamics [16,17]. However, many of these property predictions require experimental verification [3]. Therefore, a detailed characterisation of the atomic structure and surface chemistry of MXene and how they affect the electrical, thermoelectric, magnetic and other properties are highly valuable to the current research progress. It will provide useful data for the development of computational models to predict the most promising compounds. A greater understanding of catalytic and electrocatalytic properties and the ion dynamics between MXene sheets will enable further advancements in increased energy storage, and cycle life in battery and supercapacitor applications. In terms of mechanical properties, mechanical characterisation of MXene to determine their intrinsic mechanical properties will leads to more advanced and effective structural and multifunctional composites with MXene layers.

The majority of experimental studies conducted on MXene utilise scanning electron microscopy (SEM), transmission electron microscopy (TEM) and X-ray powder diffraction (XRD). These techniques do not provide data on the magnetic properties of a material. Small-Angle Neutron Scattering (SANS) enables precise characterisation of dimensions of the MXene, and has the potential to probe the magnetic structure. Importantly, SANS is capable of determining the structure of materials containing light elements (such as hydrogen), and none of the characterization techniques previously mentioned is sensitive to hydrogen present in the MXene terminations, which is critical for understanding surface and interlayer nature in this new class of materials [18]. There are several neutron scattering studies for nanomaterials that have investigated the ligand and light species at the surface of oxide and metal nanoparticles [19-21]. There has been a study that adopted neutron diffraction to provide new data on light atoms species at the surfaces and interfaces of $TiC_2T_x$ MXenes. It led to the development of a novel atomistic model for the prediction of physical, chemical and applied properties of $Ti_3C_2$ based MXene [22]. In summary, SANS is a powerful method to investigate the large-scale structure of the nanometre ($10^{-9}$ m) to the micrometre ($10^{-6}$ m) length scale [23,24] and is often the only method to obtain structural information on the bulk material (average size, shape, orientation, etc.). Furthermore, the length scale can be further reduced by applying Ultra-small-angle scattering (USANS) for objects of size 10 μm and below. However, anything >30 μm is infinite as it is out of size range by USANS. SANS have superior penetration capability due to the selective absorption and scattering cross-section of neutrons across the periodic table and can often be applied in situ, unlike microscopy where most of the time samples are modified.

In light of the aforementioned knowledge gaps, this study will examine the structural morphology of MXene and provide a high fidelity characterisation of the material properties. This includes physical properties such as the thickness and the interlayer gaps of the MXene nanosheet. This experiment will provide a deeper understanding of the fundamentals that contribute to MXene's effectiveness as a material for energy storage and flame retardancy. The specific objectives of this study are as follows:

1 Understanding the morphological structure and elemental distribution of the chemical etched MXene nanosheets through various experimental characterisation methods, including SEM, TEM and X-ray Photoelectron Spectroscopy (XPS); and
2 Obtain information regarding the structural architecture of as prepared $Ti_3C_2$ MXene, and investigate the influence of temperature on these structural parameters through the analysis of SANS data from $Ti_3C_2$ MXene at temperatures between 20 °C and 60 °C. This study is expected to pave the way for future studies where more samples, temperatures and in-situ setups will be used.

## 2. Material and methods

### 2.1. Materials

Titanium aluminium carbide ($Ti_3AlC_2$) was purchased from the Hello Nano Technology Co. Ltd., (Changchun, China). Lithium fluoride (LiF) was purchased from the Aladdin Reagent Co. Ltd., China. Hydrochloric acid (HCl, 36% - 38%) were purchased from the Sinopharm Chemical Reagent Co. Ltd., (Shanghai, China). Cetrimonium bromide (CTAB) was purchased from Sigma Aldrich (Australia). Deuterium oxide ($D_2O$, 99.8 atom % D) was purchased from Chemsupply (Australia).

### 2.2. Synthesis

The preparation of $Ti_3C_2$ nanosheets was conducted by etching $Ti_3AlC_2$ using LiF and HCl followed by exfoliation based on previous works [25]. Diluted HCl was prepared first by adding 2.5 ml distilled water into a test tube followed by 7.5 ml 9 M HCl. Then, 0.5 g LiF and 0.5 g $Ti_3AlC_2$ were added to the acid solution. The etching process was conducted at a temperature of 40°C with magnetic stirring for 48 hours to remove the interlayer of Al. The reaction mixture was then centrifuged

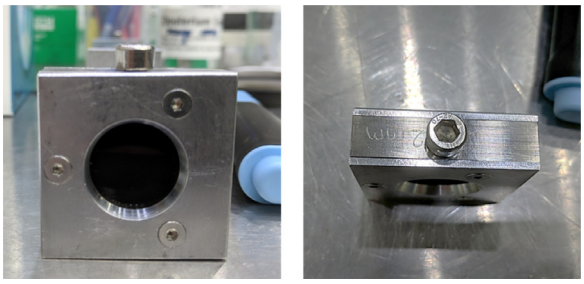

**Fig. 2.** Image of the $Ti_3C_2/D_2O$ dispersion in the sample cell.

at 9500 rpm (Eppendorf Centrifuge 5810) for 5 minutes to recover the sediments by decanting the supernatant. The centrifugation process was repeated with fresh deionised water until the pH value of the mixture become neutral. The exfoliation process was conducted by using 120 ml of deionised water to flush the centrifuged material into a beaker for ultra-sonication for 30 minutes. The suspension was then centrifuged again for 5 minutes under 4000 rpm to remove the unexploited layered $Ti_3C_2$ powders. Finally, a colloidal suspension containing single or few-layered $Ti_3C_2$ nanosheets was obtained. The $Ti_3C_2$ suspension was obtained by diluting the as-prepared $Ti_3C_2$ nanosheet with the deionised water until the concentration was 1 mg/ml.

### 2.3. Characterisation

In addition to the small-angle neutron scattering (SANS), the $Ti_3C_2$ nanosheets were characterised by SEM, TEM and XPS. SEM analysis was conducted on a Hitachi SU8010 SEM (Tokyo, Japan) with an acceleration voltage of 10 kV. TEM was carried out using a JEOL JEM-2100 instrument with an acceleration voltage of 200 kV. The XPS was conducted on a K-alpha X-ray spectrometer (Thermofisher Scientific Company) with Al source.

### 2.4. Small-angle neutron scattering

SANS is a well-established and powerful technique used to study the nanostructure of various materials in size range of 1 - 1000 nm. In this work, the SANS were conducted on the BILBY SANS instrument [26] in the Australian Centre for Neutron Scattering (ACNS), located at the Australian Nuclear Science and Technology Organisation (ANSTO). The instrument was run in monochromatic mode, at a neutron wavelength of $\lambda = 6.0$ Å and a corresponding wavelength resolution of $\Delta\lambda / \lambda = 0.1$. The three detector banks were positioned at ~8.8 m, 2.7 m and 1.7 m from the sample giving access to a $Q$-range of ~0.01 - 0.4 $Å^{-1}$. This corresponds to a size range from 6300 Å (63 nm) to 16 Å (1.6 nm), which are appropriate for probing the internal structure and separation of lamellar structures. Data were placed on an absolute scale against the direct beam intensity using Mantid [27], and reduced to I($Q$) vs $Q$, where $Q = \frac{4\pi}{\lambda}\sin(\theta)$, $\lambda$ is the wavelength and $2\theta$ is the scattering angle. The $I(q)$ vs $q$ data were corrected for solvent scattering by subtraction of scattering from an appropriate blank. All samples were maintained at 20, 30, 40, 50 or 60°C during measurement by a temperature controlled sample changer.

#### 2.4.1. Preparation of samples

All the MXene samples were prepared in $D_2O$ solution at a concentration of 1.3 wt%. Samples were mounted in a 2 mm path length demountable cell with quartz windows in an Ar glovebox as illustrated in **Fig. 2**. In-situ SANS was then used to determine the thickness of the nanosheets, and the interstitial gaps between the layers. The scattering length density of the $Ti_3C_2$ nanosheet is ~0.3 × $10^{-6}$ $Å^{-2}$, and the use of $D_2O$ (scattering length density of 6.34 × $10^{-6}$ $Å^{-2}$) as the supporting solvent maximises the contrast of the nanosheet in solution. The use of $H_2O$ (scattering length density of -0.56 × $10^{-6}$ $Å^{-2}$) would result in a lower nanosheet contrast, thus, less scattering. This distinct difference in scattering length between the two isotopes of hydrogen, protium and deuterium is extremely valuable for the study of hydrogen-containing materials and forms the basis of a method known as contrast variation. Neutrons are scattered by nuclei, and the extent of this scattering is dependent on the composition of the nucleus, while for X-ray radiation, it is dependent on the electronic structure of the target atom [28].

#### 2.4.2. Test environment and conditions

At a fixed ambient temperature, the scattering profile of the specimen was measured at ambient pressure. - The same experiment was repeated at temperatures ranging from 20 °C to 60 °C.

#### 2.4.3. Analytical method and data treatment

The background corrected $I(Q)$ (or differential macroscopic scattering cross-section as the intensity data are on an absolute scale), vs the scattering vector $Q$, were analysed using SasView, Small-Angle Scattering Analysis Software Package version 5 [29].

#### 2.4.4. SANS Data Analytical Model

To obtain useful information regarding the structure, size and shape of the MXene nanosheets from the experimental data, the "Lamella" model was adopted based on our understanding of the layered Ti/C structure. As $Ti_3C_2$ is two-dimensional materials with stacking layers of titanium and carbon. It can be assumed that the structure of the testing samples will exhibit features of the lyotropic lamellar phases [30,31]. For a lyotropic lamellar phase where a random distribution in solution is assumed. The scattering length density (SLD) of the head region (the functionalised surface) is taken to be different from the SLD of the tail region (the bulk $Ti_3C_2$ nanosheet). The scattering intensity $I(Q)$ is given by:

$$I(Q) = 2\pi \frac{scale}{2(\delta_H + \delta_T)} P(Q) \frac{1}{Q^2} \tag{1}$$

The form factor $P(Q)$ is:

$$P(Q) = \frac{4}{Q^2}\left\{\Delta\rho_H\left[\sin\left[Q(\delta_H + \delta_T)\right] - \sin\left(Q\delta_T\right)\right] + \Delta\rho_T \sin\left(Q\delta_T\right)\right\}^2 \tag{2}$$

where $\delta_T$ is the length tail, $\delta_H$ is the length head, $\Delta\rho_H$ is the head contrast and $\Delta\rho_T$ is the tail contrast. The total thickness of the lamellar sheet is $2(\delta_T + \delta_H)$. A figure illustration of the lamella structural features is shown in **Fig. 3**

## 3. Results and Discussion

### 3.1. Morphology of MXene via SEM/TEM

SEM and TEM images of $Ti_3C_2$ was acquired to visualise the layered structure of the nanosheets after the etching process. In **Fig. 4(a)**, the multiple nanoflakes visible in the image demonstrates that the MXene was effectively etched out from its MAX phase with the removal of the Al layer. Sequentially, it can be observed in **Fig. 4(b)** that the resulting nanosheets are ultrathin and multi-layered with clear sharp edges, confirming the quality of the fabrication procedures. Previous studies also showed that the lateral size distribution of few layers of $Ti_3C_2$ ranged from 0.1 $\mu$m to 1.3 $\mu$m, with most in the 0.3 - 0.5 $\mu$m size range [25]. **Fig. 4(c)** and **(d)** show the TEM images of the $Ti_3C_2$ sample. According to the figure, several layered nanosheets can be found with edges positioned at the centre of the image. From **Fig. 4(c)**, it is found that the nanosheets are nearly transparent, where each layer (i.e. Ti layer or C layer) of one single $Ti_3C_2$ sheet is visible. Based on the higher magnification image (**Fig. 4(d)**), the thickness of one single layer $Ti_3C_2$ can be estimated to be around 1 - 2 nm. Overall, the high quality $Ti_3C_2$ ultrathin nanosheets can be formed via the etching process using hydrofluoric acid and lithium fluoride. Provided that the morphological structure of MXene observed are layered, we propose the "lamella" model should

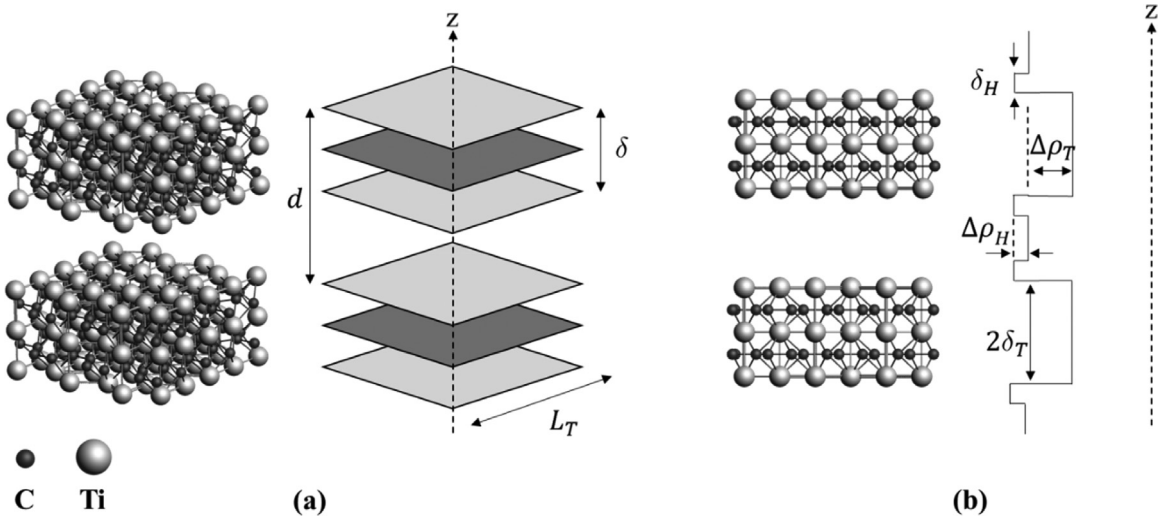


**Fig. 3.** (a) Geometric model of a lyotropic lamellar phase; the bilayers has thickness $\delta$; the bilayers are stacked along the z-direction with period $d$. (b) Schematic scattering length density profile along the normal to the bilayer z in SANS.

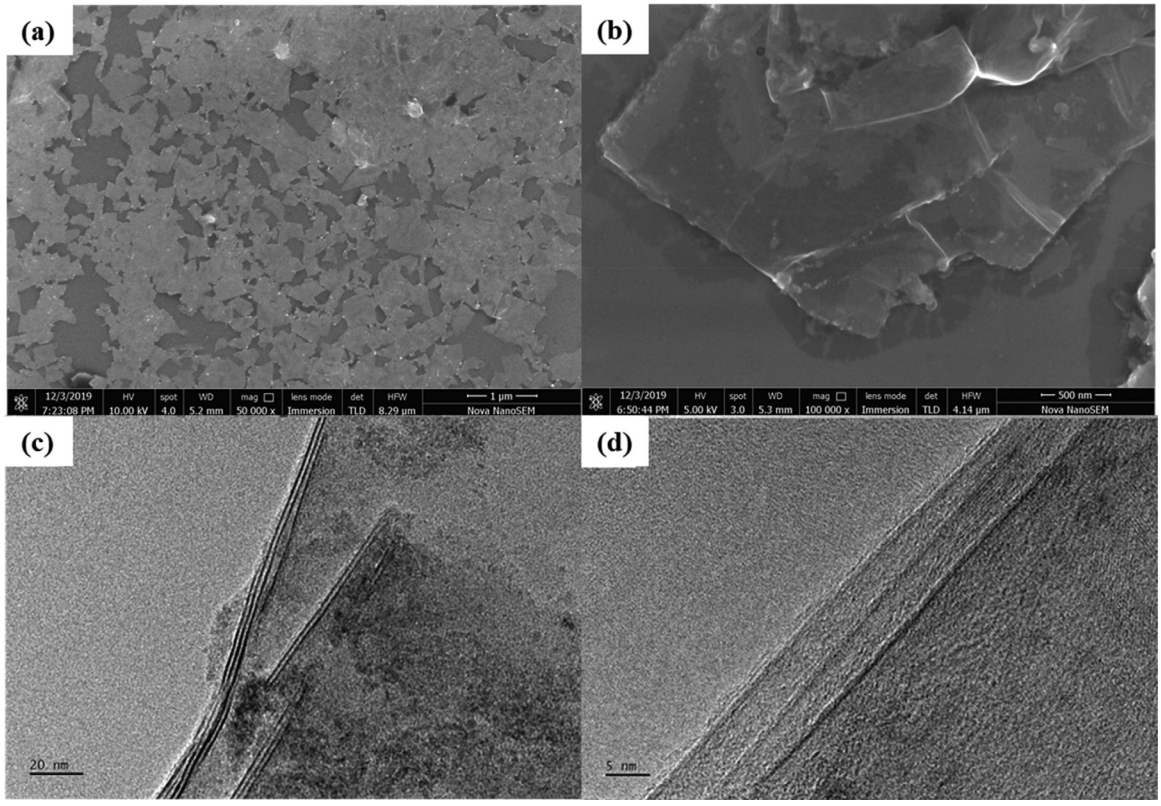


**Fig. 4.** SEM (a and b) and TEM (c and d) images of funtionalised $Ti_3C_2$ nanosheets at various magnification

be adopted to analyse the SANS data. Accordingly, the average dimensions, shape and configuration of the etched $Ti_3C_2$ nanosheets would be realised.

### 3.2. Molecular structure and surface elemental composition of MXene

In order to investigate the element composition of the surface functional groups of the chemically etched MXene, we conducted X-ray photoelectron spectroscopy (XPS) characterisation on the as prepared $Ti_3C_2$ samples, as the surface topology would affect the scattering pattern in the SANS experiment. X-ray photoelectron spectroscopy (XPS), also known as electron spectroscopy for chemical analysis (ESCA), is a technique for analysing the surface chemistry of a material. XPS can measure the elemental composition, empirical formula, chemical state and electronic state of the elements within a material. The XPS analysis was conducted to study the surface elemental compositions. According to the **Fig. 5(a)**, Li 1s, Cl 2p, C 1s, Ti 2p, O 1s, Ti 2s and F 1s peaks were identified at around 57.03, 199.08, 284.28, 454.86, 529.47, 562.08, and 684.85 eV [32], where some of the peaks can be attributed to the fabrication etching process (i.e. lithium, chloride and fluoride peaks). By observing in high-resolution XPS spectra, the C 1s spectrum displays four main peaks of $Ti_3C_2$, C-C, C-O and C=O centred at approximately 281.23, 284.04, 285.21 and 288.21 eV, respectively (**Fig. 5(b)**) [33]. Ti

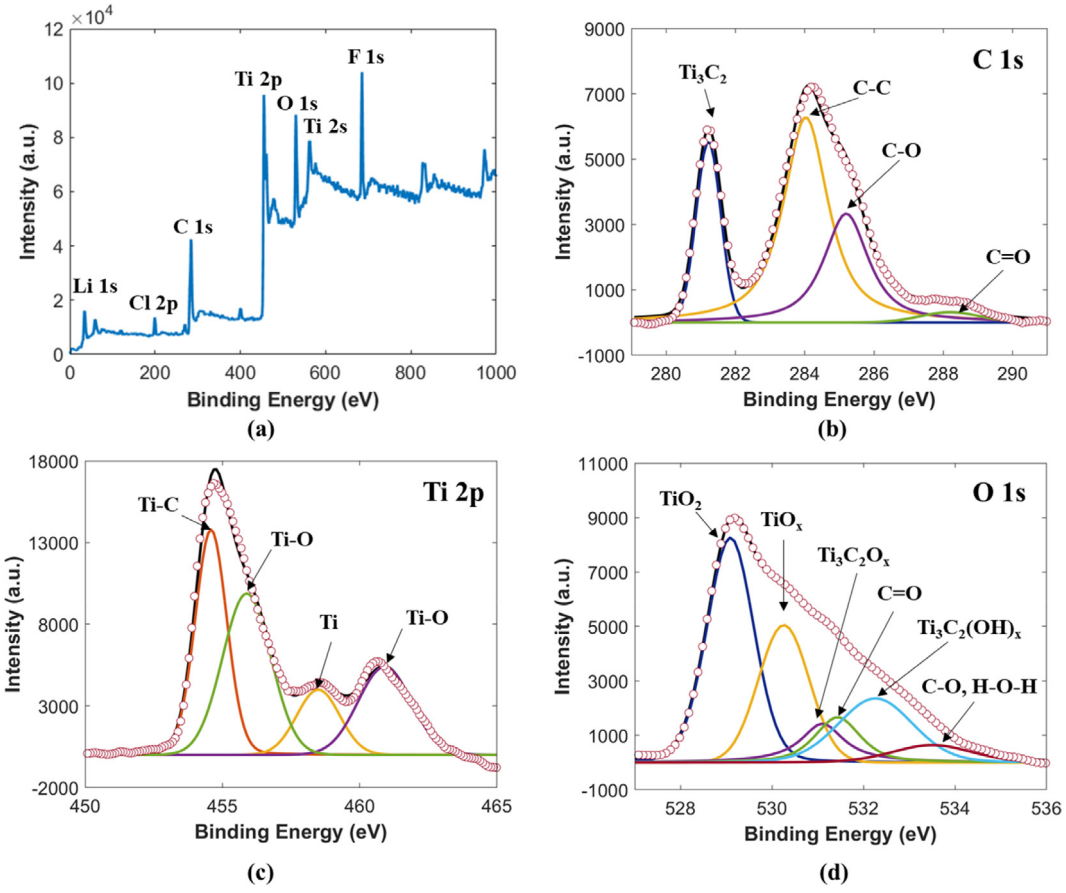


**Fig. 5.** (a) Survey XPS spectrum (b) C 1s spectra (c) Ti 2p spectra and (d) O 1s spectra of $Ti_3C_2$ nanosheets.

2p spectrum (**Fig. 5(c)**) was found to be composed of Ti-C (454.58 eV) and Ti-O (455.88 eV) peaks at 2p 3/2 orbital, and Ti (II) (458.49 eV) and Ti-O (460.91 eV) peaks at 2p 1/2 orbital [34], indicating the existence of -OH termination groups on the surface of Ti [35]. In addition, the high-resolution O 1s spectrum can be deconvoluted into $TiO_2$, $TiO_x$, $Ti_3C_2O_x$, C=O, $Ti_3C_2(OH)_x$ and C-O, H-O-H peaks at 529.09, 530.26, 531.10, 531.43, 532.26 and 533.50 eV, where oxygen-containing functional groups are confirmed on the surface of the $Ti_3C_2$ nanosheets [36].

### 3.3. Small-angle neutron scattering for MXene

The MXene samples were prepared in $D_2O$ solutions at a concentration of 1.3 wt% and exposed to the neutron beam at temperatures ranges from 20 °C to 60 °C. These experiments were performed to study (i) the morphological structure of the prepared $Ti_3C_2$ nanosheets and (ii) the influence of temperature on the $Ti_3C_2$, which may be caused by surface oxidation [37]. Unlike previous techniques (i.e. SEM, TEM, XPS), which mainly probe the surface of the samples, SANS can characterize the assembly, dispersion, alignment, as well as internal structures of nanoscale materials. **Fig. 6(a)** shows the SANS intensity profiles for $Ti_3C_2$ at temperatures from 20 °C to 60 °C, subtracted from the $D_2O$ solution background. The $Q$ range is 0.01 - 0.39 $Å^{-1}$. Generally, different structural information can be obtained from different $Q$ regions. At low-$Q$, the $I(Q)$ intensity yields information on large length scale structural features such as geometry and size of the sample (i.e. molecular weight, polydispersity, topology, and fraction dimensions). While high-Q yields information on smaller length scale surface features such as surface roughness, fractal nature of the surface and the crystallinity of the sample [38,39]. From **Fig. 6(a)**, the intensity profile of $Ti_3C_2$ is essentially unchanged by temperature, especially in the $Q$ regions < 0.1 $Å^{-1}$. In the high-$Q$ regions ($Q$ > 0.1 $Å^{-1}$), the intensity slightly increased with increasing temperature. Thus, the structural dimensions of the $Ti_3C_2$ nanosheets remain constant at temperatures between 20 to 60 °C.

Model-independent analysis consisting of firstly, a power-law fit followed by a correlation function analysis [40] was performed on the SANS data to extract useful structural information before applying more geometry-specific models. The model-independent methods require no a priori knowledge about the sample, and most importantly, no experimenter bias of assumed structure [41]. The power-law data fits are illustrated in **Fig. 6(b)** with the extracted parameters for each dataset listed in **Table 1**. An overall good fit was achieved from the power-law functions, and the results indicate the power ranges from 2.2668 - 2.2990. A value of ~2 is expected for thin sheets, thus the results are consistent with the thin lamella structure observed from previous experimental characterisation.

The correlation function is the Fourier transform of the scattering curve and may be analysed in terms of an ideal lamellar morphology [42-44] to obtain structural parameters describing the sample. The parameters that may be obtained from the correlation analysis includes the long period ($L_p$) which is also known as the Bragg spacing $d$ or lamellar repeat distance [45], average hard block thickness ($L_c$), average core thickness ($D_0$), polydispersity and the local crystallinity ($L_c/L_p$). In addition, an interface distribution function (IDF) can also be calculated, which represents a superposition of thickness distributions from all the contributing lamellae [46]. The correlation function analysis is performed in three stages: (i) extrapolation of the scattering curve to $Q = 0$ and $Q = \infty$, (ii) calculation of the Fourier Transform of the data to determine the correlation function and (iii) interpretation of the correlation function assuming the sample conforms to an ideal lamellar morphology. The low-$Q$ range is extrapolated to $Q = 0$ with the Guinier

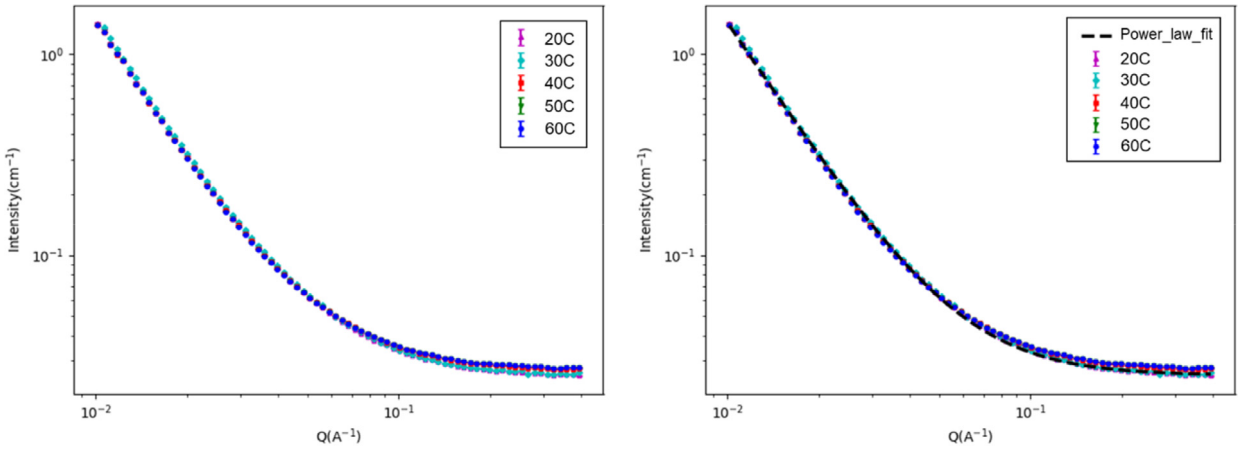


**Fig. 6.** Scattering intensity profile of (a) the $Ti_3C_2$ samples at temperatures from 20 °C to 60 °C subtracted from the $D_2O$ solution background and (b) power-law fit of the scattering data.

**Table. 1**
Summary of structural parameters from power-law fit of $Ti_3C_2$ samples

| Parameter | 20C | 30C | 40C | 50C | 60C | Average |
|---|---|---|---|---|---|---|
| scale | 4.07E-05 | 4.22E-05 | 3.88E-05 | 3.49E-05 | 3.49E-05 | 3.83E-05 |
| background | 2.53E-02 | 2.54E-02 | 2.70E-02 | 2.75E-02 | 2.75E-02 | 2.65E-02 |
| power | 2.269 | 2.267 | 2.274 | 2.299 | 2.299 | 2.282 |

function:

$$I(Q) = A.e^{(B.Q^2)} \tag{3}$$

While the high-$Q$ range data are extrapolated to $Q = \infty$ with the Porod function:

$$I(Q) = K.Q^{-4}.e^{(-\sigma^2.Q^2)} + Bg \tag{4}$$

where $B$ is proportional to a radius of gyration, $\sigma$ describes the width of the neutron scattering length density profile at the interface between the crystalline and amorphous regions. It is a measure of how abruptly the SLD changes between the quasi-lamellar regions. $Bg$ is a $Q$-independent background level. The factors $A$ and $K$ are scaling coefficients. Subsequently, the discrete cosine transform was performed on the extrapolated data to calculate the 1D correlation function expressed as:

$$\Gamma_1(x) = \frac{1}{Q^*}\int_0^\infty I(Q)Q^2\cos(Qx)dQ \tag{5}$$

where $Q^*$is the scattering (Porod) invariant. The 3D correlation function is calculated as:

$$\Gamma_3(x) = \frac{1}{Q^*}\int_0^\infty I(Q)Q^2\frac{\sin(Qx)}{Qx}dQ \tag{6}$$

In this study, the low-$Q$ range was set to range from 0.0 – 0.012 $Å^{-1}$ and the upper-$Q$ range was set to 0.12 – 0.25 $Å^{-1}$. The extrapolation prevents truncation effects in the Fourier transformation. Meanwhile, the important structural data are extracted from the experimental data in the range ~0.01-0.25 $Ang^{-1}$. While the range is somewhat arbitrary, it covers most of the measured $Q$-range and closely corresponds to lengths spanned by the thickness than the other dimensions of the sheet. Even if USANS or Bonse-Hart double-crystal diffractometer (DCD) data had have been available, the lower-$Q$ range would have been set to a very similar (if not identical range). Thus, additional USANS experiments would not have provided useful information regarding the thickness of the sheets. The correlation function analysis is illustrated in **Fig. 7** and the list of extrapolated parameters for the $Ti_3C_2$ samples from 20 °C to 60 °C are detailed in **Table 2**. The background ( $\underline{Bg}$) source was calculated to be approximately 2.60E-02 to 2.8E-02. Overall, there are very little variations in the 1D and 3D correlation functions for $Ti_3C_2$ at temperatures from 20 °C to 60 °C (**Fig. 7 (b), (d)**). In terms of the extrapolated structural parameters, the long period ($L_p$) for the $Ti_3C_2$ nanosheet ranged between 32.1 and 33.1 Å. The average hard block thickness, $L_c$ and soft block thickness $L_a$ varied from 11.4 to 11.8 Å and from 20.3 to 21.5 Å, respectively. The variations in $L_p$, $L_c$ and $L_a$ among samples under temperatures between 20 °C and 60 °C were within 2 Å, which may fall within the uncertainty range of the experimental errors. The results suggest that at this temperature range, it does not affect the structure of the $Ti_3C_2$ nanosheets. Nevertheless, this study provides information regarding the lamellar architecture in the sample sets. The structure of $Ti_3C_2$ nanosheets consists of layers of transition metal carbides in a multilayer lamellas morphology with interstack gaps [47]. Therefore, the hard block thickness or the crystalline thickness of 11.4 – 11.8 Å (i.e. 1.14 – 1.18 nm) from the SANS data can be interpreted to be the thickness of a single layer of $Ti_3C_2$. Subsequently, the soft block thickness of 20.3 – 21.5 Å (2.03 – 2.15 nm) can be taken to be an approximation of the interstacking layer gaps within the $Ti_3C_2$ samples. Under these assumptions, the magnitude of the extrapolated thicknesses was in agreement with other experimental observations [7,48].

### *3.4. Characterisation of MXene dimensional parameters using Lamella model*

The SANS results were curve-fitted using the lamella model to further study the key structural parameters for the $Ti_3C_2$ samples at various temperature. Under the lamella model framework, there are a total of five parameters for optimisation to curve-fit against the experimental data. The parameters including scale factor or volume fraction (scale), source background (background), thickness, scattering length density (SLD), and solvent scattering length density (SLD_solvent). The parameter scattering length density of the solvent (SLD_solvent) was set to 6.34E-06 $Å^{-2}$ according to the background $D_2O$ solvent. The SLD of the $Ti_3C_2$ layers was calculated to be around 0.29E-06 $Å^{-2}$ assuming a den-

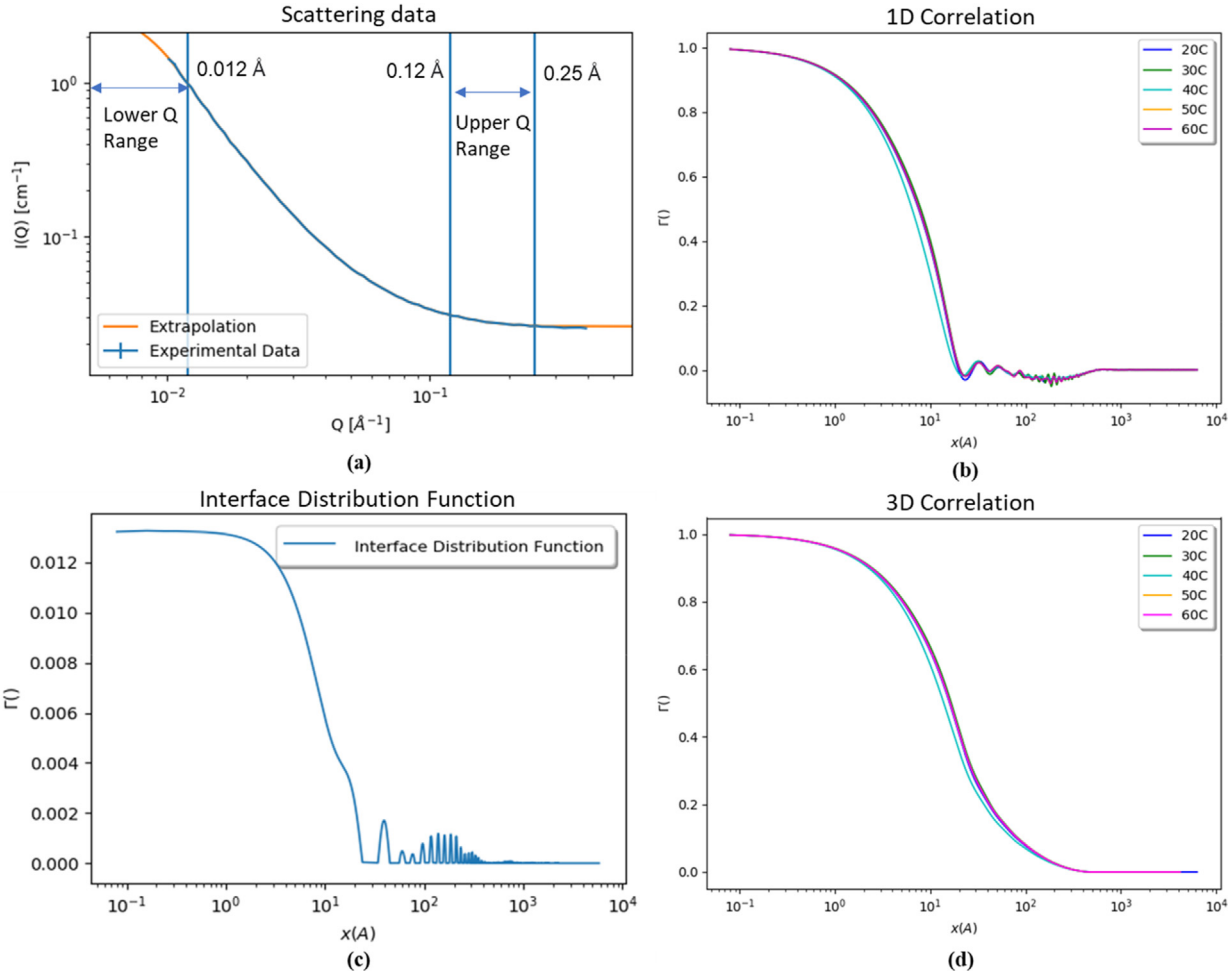


**Fig. 7.** Correlation function analysis of $Ti_3C_2$ scattering data at 20 °C. (a) scattering intensity, *I(Q)* profile illustrating the lower and upper *Q* range. (b) 1D correlation function. (c) the extrapolated interface distribution function (IDF) and (d) 3D correlation function from the correlation analysis.

**Table. 2**
Summary of structural parameters from correlation function analysis of $Ti_3C_2$ samples

| Parameter | | 20C | 30C | 40C | 50C | 60C |
|---|---|---|---|---|---|---|
| Guinier | A | 1.38 | 1.42 | 1.36 | 1.31 | 1.31 |
| | B | -9.83E+03 | -9.88E+03 | -9.94E+03 | -9.50E+03 | -9.50E+03 |
| Porod | K | 1.16E-06 | 1.10E-06 | 1.13E-06 | 1.07E-06 | 1.18E-06 |
| | $\sigma$ | 1.65E-07 | 2.00E-05 | 4.94E-11 | 1.27E-09 | 2.04E-05 |
| background | | 2.60E-02 | 2.63E-02 | 2.77E-02 | 2.81E-02 | 2.79E-02 |
| long period (Å) | | 33.1 | 32.1 | 32.6 | 32.3 | 32.3 |
| average hard block thickness (Å) | | 11.6 | 11.8 | 11.4 | 11.6 | 11.6 |
| average soft block thickness (Å) | | 21.5 | 20.3 | 21.2 | 20.7 | 20.7 |
| polydispersity | | 0.0369 | 0.0215 | 0.0374 | 0.0238 | 0.0238 |
| average core thickness (Å) | | 1.83 | 1.83 | 1.75 | 1.83 | 1.83 |
| local crystallinity | | 0.349 | 0.369 | 0.351 | 0.359 | 0.359 |

sity of 2.5 g $cm^{-3}$. While the surface layer (i.e. O, OH and F terminations) [49-51] will affect the SLD of the particle, they are localised to the surface, and layer thickness is small relative to the $Ti_3C_2$ layer. Therefore it will have very low contrast in $D_2O$, and thus in the model, the SLD of the $Ti_3C_2$ was fixed. The rest of the parameters were automatically adjusted based on the SasView built-in algorithm. The background source was set to a range between 2.6E-02 – 2.9E-02, and the initial approximation of the thickness was set to 32 Å which is equal to the long period ($L_p$) from the correlation function analysis.

Fig. 8 shows the comparisons between the numerical fitted curve versus the experimental data, and the optimised model parameters are shown in Table 3. Overall, the model achieved a good fit with the experimental data, which provides further evidence for the thickness of the $Ti_3C_2$ samples. The thickness ranged from 29.14 - 32.27 Å, which are comparable with the long period thickness from the correlation analysis. Furthermore, the optimised background sources are also consistent with all previous results. Interestingly, the lamella model results indicate that from 20 °C to 40 °C, the thickness is consistently around 29 Å, while increasing to 50 °C and 60 °C leads to an increase in thickness from 29 Å to 32 Å. In summary, the results indicate that $Ti_3C_2$ nanosheets are relatively stable at the temperature range from 20 to 60 °C, and there was a slight increase in the thickness of the $Ti_3C_2$ layers when heat was exerted to the sample solutions.

**Table. 3**
Lamella model parameters for $Ti_3C_2$ samples ranging from 20 - 60 °C.

| Parameter | 20C | 30C | 40C | 50C | 60C | Average |
|---|---|---|---|---|---|---|
| scale | 1.77E-04 | 1.82E-04 | 1.69E-04 | 1.56E-04 | 1.56E-04 | 1.68E-04 |
| background | 2.64E-02 | 2.65E-02 | 2.80E-02 | 2.85E-02 | 2.85E-02 | 2.76E-02 |
| thickness (Å) | 29.14 | 29.01 | 29.76 | 32.27 | 32.27 | 30.49 |
| SLD ($10^{-6}Å^{-2}$) | 0.290 | 0.290 | 0.290 | 0.290 | 0.290 | 0.290 |
| SLD_solvent ($10^{-6}Å^{-2}$) | 6.340 | 6.340 | 6.340 | 6.340 | 6.340 | 6.340 |

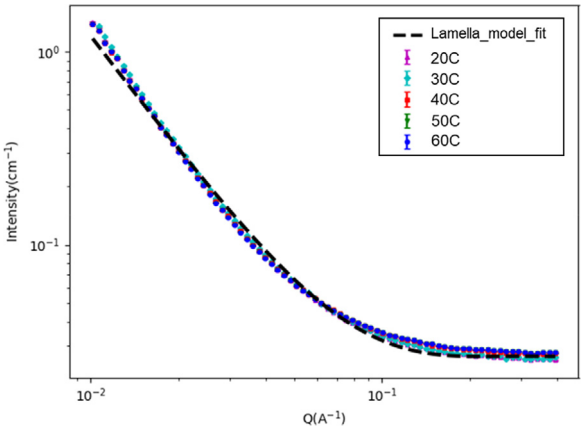


**Fig. 8.** Lamella model curve fit of the scattering intensity profile of 1.3 wt% $Ti_3C_2$ samples at temperatures from 20 °C to 60 °C subtracted from the $D_2O$ solution background.

## 4. Conclusion

In this article, the morphological structure of MXene ($Ti_3C_2$) nanosheets were investigated with the application of small-angle neutron scattering (SANS) combined with several complementary techniques, such as scanning electron microscopy (SEM), Transmission Electron Microscopy (TEM) and X-ray Photoelectron Spectroscopy (XPS). The $Ti_3C_2$ nanosheets were synthesised via the etching process using hydrofluoric acid and lithium fluoride. The SEM results showed that the Ti3C2 nanosheets are ultrathin and multi-layered with clear sharp edges which are similar to lamella structure. Based on the higher magnification images, the thickness of one single layer Ti3C2 can be estimated to be around 1 - 2 nm. A series of model-independent statistical analysis (i.e. power-law and correlation function analysis) and 1D model curve-fitting (i.e. lamella model) was performed to extrapolate key information from the SANS data regarding the structural architecture of the $Ti_3C_2$ nanosheets and investigate the influence of temperature on these structural parameters. From the correlation function analysis, the hard block thickness or the crystalline thickness of 11.4 – 11.8 Å (i.e. 1.14 – 1.18 nm) from the SANS data can be interpreted to be the thickness of a single layer of $Ti_3C_2$. Subsequently, the soft block thickness of 20.3 – 21.5 Å (2.03 – 2.15 nm) can be taken to be an approximation of the interstacking layer gaps within the MXene samples. This adds up to a total layer thickness of approximately 32 Å (3.2 nm), which was consistent with the 29 Å to 32 Å range obtained through the shape-dependent lamella model and are aligned with SEM/TEM observations. Furthermore, the lamella model results indicate that from 20 °C to 40 °C, the thickness is consistently around 29 Å, while increasing to 50 °C and 60 °C leads to an increase in thickness from 29 Å to 32 Å. There were no clear indications of oxidation effects or changes to the scattering length density of the sample. In summary, the dimensions, shape and configuration of the etched $Ti_3C_2$ nanosheets were successfully characterised via SANS analytical methods. The structure of $Ti_3C_2$ nanosheets consists of layers of transition metal carbides in a multilayer lamellas morphology with interstack gaps. The results indicate that $Ti_3C_2$ nanosheets are relatively stable at the temperature range from 20 to 60 °C, and there was a slight increase in the thickness of the $Ti_3C_2$ layers when the temperature range increased to between 50 to 60 °C.

## Declaration of Competing Interest

None.

## Acknowledgement

This research is sponsored by the Australian Research Council (ARC Industrial Training Transformation Centre IC170100032) and the Australian Government Research Training Program Scholarship. We also acknowledge and express our gratitude for the support by ANSTO in providing the BILBY SANS beamtime (ACNS Neutron Beam Instrument Proposal P7332). All financial and technical support is greatly appreciated. This work benefited from the use of the SasView application, originally developed under NSF Award DMR-0520547. SasView also contains code developed with funding from the EU Horizon 2020 programme under the SINE2020 project Grant No 654000.

## References

[1] B Anasori, ÜG. Gogotsi, 2D metal carbides and nitrides (MXenes), Springer, 2019.
[2] NK Chaudhari, H Jin, B Kim, D San Baek, SH Joo, K Lee, MXene: an emerging two-dimensional material for future energy conversion and storage applications, J. Mater. Chem. A 5 (47) (2017) 24564–24579.
[3] B Anasori, MR Lukatskaya, Y. Gogotsi, 2D metal carbides and nitrides (MXenes) for energy storage, Nat. Rev. Mater. 2 (2017) 16098.
[4] M Shekhirev, CE Shuck, A Sarycheva, Y. Gogotsi, Characterization of MXenes at every step, from their precursors to single flakes and assembled films, Prog. Mater Sci. (2020) 100757.
[5] L Verger, C Xu, V Natu, H-M Cheng, W Ren, MW. Barsoum, Overview of the synthesis of MXenes and other ultrathin 2D transition metal carbides and nitrides, Curr. Opin. Solid State Mater. Sci. 23 (3) (2019) 149–163.
[6] L Verger, V Natu, M Carey, MW. Barsoum, MXenes: An Introduction of Their Synthesis, Select Properties, and Applications, Trends in Chem. 1 (7) (2019) 656–669.
[7] B Yu, B Tawiah, L-Q Wang, AC Yin Yuen, Z-C Zhang, L-L Shen, et al., Interface decoration of exfoliated MXene ultra-thin nanosheets for fire and smoke suppressions of thermoplastic polyurethane elastomer, J. Hazard. Mater. 374 (2019) 110–119.
[8] R Bian, R Lin, G Wang, G Lu, W Zhi, S Xiang, et al., 3D assembly of Ti3C2-MXene directed by water/oil interfaces, Nanoscale 10 (8) (2018) 3621–3625.
[9] X Sang, Y Xie, M-W Lin, M Alhabeb, KL Van Aken, Y Gogotsi, et al., Atomic Defects in Monolayer Titanium Carbide (Ti3C2Tx) MXene, ACS Nano 10 (10) (2016) 9193–9200.
[10] LH Karlsson, J Birch, J Halim, MW Barsoum, Persson POÅ, Atomically resolved structural and chemical investigation of single MXene sheets, Nano Lett. 15 (8) (2015) 4955–4960.
[11] JL Hart, K Hantanasirisakul, AC Lang, B Anasori, D Pinto, Y Pivak, et al., Control of MXenes' electronic properties through termination and intercalation, Nat. Commun. 10 (1) (2019) 1–10.
[12] K Maleski, CE Ren, M-Q Zhao, B Anasori, Y. Gogotsi, Size-dependent physical and electrochemical properties of two-dimensional MXene flakes, ACS Appl. Mater. Interfaces 10 (29) (2018) 24491–24498.
[13] B Anasori, Y Xie, M Beidaghi, J Lu, BC Hosler, L Hultman, et al., Two-dimensional, ordered, double transition metals carbides (MXenes), ACS nano 9 (10) (2015) 9507–9516.
[14] R Meshkian, L-Å Näslund, J Halim, J Lu, MW Barsoum, J. Rosen, Synthesis of two-dimensional molybdenum carbide, Mo2C, from the gallium based atomic laminate Mo2Ga2C, Scr. Mater. 108 (2015) 147–150.
[15] M Kurtoglu, M Naguib, Y Gogotsi, MW. Barsoum, First principles study of two-dimensional early transition metal carbides, Mrs Commu. 2 (4) (2012) 133–137.
[16] VN Borysiuk, VN Mochalin, Y. Gogotsi, Molecular dynamic study of the mechanical properties of two-dimensional titanium carbides Tin+ 1Cn (MXenes), Nanotechnology 26 (26) (2015) 265705.

[17] L Li, T Zhang, Y Duan, Y Wei, C Dong, L Ding, et al., Selective gas diffusion in two-dimensional MXene lamellar membranes: insights from molecular dynamics simulations, J. Mater. Chem. A 6 (25) (2018) 11734–11742.
[18] H-W Wang, M Naguib, K Page, DJ Wesolowski, Y. Gogotsi, Resolving the structure of ti3c2t x mxenes through multilevel structural modeling of the atomic pair distribution function, Chem. Mater. 28 (1) (2016) 349–359.
[19] SJ. Billinge, Nanoscale structural order from the atomic pair distribution function (PDF): There's plenty of room in the middle, J. Solid State Chem. 181 (7) (2008) 1695–1700.
[20] K Page, TC Hood, T Proffen, RB. Neder, Building and refining complete nanoparticle structures with total scattering data, J. Appl. Crystallogr. 44 (2) (2011) 327–336.
[21] H-W Wang, DJ Wesolowski, TE Proffen, L Vlcek, W Wang, LF Allard, et al., Structure and stability of SnO2 nanocrystals and surface-bound water species, J. Am. Chem. Soc. 135 (18) (2013) 6885–6895.
[22] H-W Wang, M Naguib, K Page, DJ Wesolowski, Y. Gogotsi, Resolving the structure of ti3c2t x mxenes through multilevel structural modeling of the atomic pair distribution function, Chem. Mater. 28 (1) (2015) 349–359.
[23] R Palm, R Härmas, E Härk, B Kent, H Kurig, M Koppel, et al., Study of the structural curvature in Mo2C derived carbons with contrast matched small-angle neutron scattering, Carbon 171 (2021) 695–703.
[24] W. Ruland, Apparent fractal dimensions obtained from small-angle scattering of carbon materials, Carbon (New York, NY) 39 (2) (2001) 323–324.
[25] B Lin, ACY Yuen, A Li, Y Zhang, TBY Chen, B Yu, et al., MXene/chitosan nanocoating for flexible polyurethane foam towards remarkable fire hazards reductions, J. Hazard. Mater. 381 (2020) 120952.
[26] A Sokolova, AE Whitten, L de Campo, J Christoforidis, A Eltobaji, J Barnes, et al., Performance and characteristics of the BILBY time-of-flight small-angle neutron scattering instrument, J. Appl. Crystallogr. 52 (1) (2019) 1–12.
[27] O Arnold, JC Bilheux, JM Borreguero, A Buts, SI Campbell, L Chapon, et al., Mantid—Data analysis and visualization package for neutron scattering and $\mu$ SR experiments, Nucl. Instrum. Methods Phys. Res. Sect. A 764 (2014) 156–166.
[28] A Lopez-Rubio, EP. Gilbert, Neutron scattering: a natural tool for food science and technology research, Trends Food Sci. Technol. 20 (11-12) (2009) 576–586.
[29] SasView. (http://www.sasview.org/).
[30] J Berghausen, J Zipfel, P Lindner, W. Richtering, Influence of water-soluble polymers on the shear-induced structure formation in lyotropic lamellar phases, J. Phys. Chem. B 105 (45) (2001) 11081–11088.
[31] Nallet F, Laversanne R, Roux DJJdPI. Modelling X-ray or neutron scattering spectra of lyotropic lamellar phases: interplay between form and structure factors. 1993;3(4):487-502.
[32] H Ao, K Qi, X Zhang, M Liu, T Zhou, S Wang, et al., A High-rate, long life and anti-self-discharge aqueous N-doped Ti3C2/Zn hybrid capacitor, Mater. Today Energy (2020) 100598.
[33] Q Fu, J Wen, N Zhang, L Wu, M Zhang, S Lin, et al., Free-standing Ti 3 C 2 T x electrode with ultrahigh volumetric capacitance, RSC Adv. 7 (20) (2017) 11998–12005.
[34] Y Wang, X Gao, L Zhang, X Wu, Q Wang, C Luo, et al., Synthesis of Ti3C2/Fe3O4/PANI hierarchical architecture composite as an efficient wide-band electromagnetic absorber, Appl. Surf. Sci. 480 (2019) 830–838.
[35] M Naguib, M Kurtoglu, V Presser, J Lu, J Niu, M Heon, et al., Two-dimensional nanocrystals produced by exfoliation of Ti3AlC2, Adv. Mater. 23 (37) (2011) 4248–4253.
[36] L Li, M Zhang, X Zhang, Z. Zhang, New Ti3C2 aerogel as promising negative electrode materials for asymmetric supercapacitors, J. Power Sources 364 (2017) 234–241.
[37] Y Lee, SJ Kim, Y-J Kim, Y Lim, Y Chae, B-J Lee, et al., Oxidation-resistant titanium carbide MXene films, J. Mater. Chem. A 8 (2) (2020) 573–581.
[38] EM. Anitas, Small-Angle Scattering from Mass and Surface Fractals, Complexity in Biological and Physical Systems-Bifurcations, Solitons and Fractals: IntechOpen, 2017.
[39] D Mildner, P. Hall, Small-angle scattering from porous solids with fractal geometry, J. Phys. D Appl. Phys. 19 (8) (1986) 1535.
[40] AJ. Ryan, SAXS correlation functions: New Software at Daresbury, Fibre Diffraction Rev. 3 (1994) 25–29.
[41] S. Kline, Reduction and analysis of SANS and USANS data using IGOR Pro, J. Appl. Crystallogr. 39 (6) (2006) 895–900.
[42] F Balta-Calleja, C. Vonk, X-ray scattering of synthetic polymers, Elsevier, Amsterdam, 1989.
[43] JT Koberstein, RS. Stein, Small-angle x-ray scattering measurements of diffuse phase-boundary thicknesses in segmented polyurethane elastomers, J. polymer sci.: polymer physics edition 21 (10) (1983) 2181–2200.
[44] GR Strobl, M. Schneider, Direct evaluation of the electron density correlation function of partially crystalline polymers, J. Polymer Sc.: Polymer Physics Edition 18 (6) (1980) 1343–1359.
[45] J Blazek, H Salman, AL Rubio, E Gilbert, T Hanley, L. Copeland, Structural characterization of wheat starch granules differing in amylose content and functional characteristics, Carbohydr. Polym. 75 (4) (2009) 705–711.
[46] W. Ruland, The evaluation of the small-angle scattering of lamellar two-phase systems by means of interface distribution functions, Colloid Polym. Sci. 255 (5) (1977) 417–427.
[47] B Anasori, MR Lukatskaya, Y. Gogotsi, 2D metal carbides and nitrides (MXenes) for energy storage, Nat. Rev. Mater. 2 (2) (2017) 16098.
[48] M Hu, H Zhang, T Hu, B Fan, X Wang, Z. Li, Emerging 2D MXenes for supercapacitors: status, challenges and prospects, Chem. Soc. Rev. 49 (18) (2020) 6666–6693.
[49] MA Hope, AC Forse, KJ Griffith, MR Lukatskaya, M Ghidiu, Y Gogotsi, et al., NMR reveals the surface functionalisation of Ti3C2 MXene, PCCP 18 (7) (2016) 5099–5102.
[50] I Persson, L-Å Näslund, J Halim, MW Barsoum, V Darakchieva, J Palisaitis, et al., On the organization and thermal behavior of functional groups on Ti3C2 MXene surfaces in vacuum, 2D Materials 5 (1) (2017) 015002.
[51] O Mashtalir, M Naguib, VN Mochalin, Y Dall'Agnese, M Heon, MW Barsoum, et al., Intercalation and delamination of layered carbides and carbonitrides, Nat. Commun. 4 (1) (2013) 1–7.